Heat transfer in an oval tube heat exchanger with different kinds of longitudinal vortex generators

Article *in* Heat Transfer Research · November 2017
DOI: 10.1615/HeatTransRes.2017018543

2 authors, including:

Alvaro A Valencia
University of Chile
76 PUBLICATIONS **1,248** CITATIONS

SEE PROFILE

Heat Transfer Research 48(18):1707–1725 (2017)

HEAT TRANSFER IN AN OVAL TUBE HEAT EXCHANGER WITH DIFFERENT KINDS OF LONGITUDINAL VORTEX GENERATORS

*Daniel Díaz & Alvaro Valencia**

Department of Mechanical Engineering, Universidad de Chile, 8370456, Santiago, Chile

*Address all correspondence to: Alvaro Valencia, Department of Mechanical Engineering, Universidad de Chile, Santiago, 8370456, Chile, E-mail: alvalenc@ing.uchile.cl

Original Manuscript Submitted: 8/9/2016; Final Draft Received: 4/25/2017

A numerical study was performed on a plate fin and oval tube heat exchanger with different kinds of longitudinal vortex generators (LVG). The influence of LVG on heat transfer and pressure drop is investigated, and eight different LVG geometries are compared: delta-type, rectangular, spoon-type, and five ellipse-shaped cases. The numerical study involves a three-dimensional steady and laminar flow and conjugate heat transfer. The results show that one longitudinal vortex (LV) is generated for each LVG for all cases except for the spoon-type case, where two LVs are generated. The results of experimental and numerical investigations were compared validation. The highest increase in heat transfer corresponds to the Delta case (14% for Re_{dh} = 720), followed by the Ellipse 1 (13%), Ellipse 2, Ellipse 5 and Rectangular (11%), Ellipse 3 (8%), and Ellipse 4 and Spoon (7%) cases. The highest increase in the pressure drop corresponds to the Ellipse 1 case (20% for Re_{dh} = 720), followed by the Delta (19%), Ellipse 2 (15%), Ellipse 5 (14%), Rectangular (13%), Ellipse 3 (11%), and Ellipse 4 and Spoon (9%) cases. The highest heat transfer rate, with the same flow power consumption, corresponds to the Delta, Rectangular, Ellipse 1, 2, and 5 cases.

KEY WORDS: *heat transfer enhancement, heat exchanger, vortex generator*

1. INTRODUCTION

Finned-tube heat exchangers are widely used in engineering applications such as heating, ventilation, air conditioning, and refrigeration. When using air, the air-side thermal resistance is the largest contributor to the overall thermal resistance; therefore, fins are used to increase the exchanging surface and enhance heat transfer in the air side. However, the extension of the fins is limited by practical and economic factors; so other strategies, such as increasing the heat transfer coefficient, are needed.

Longitudinal vortex generators (LVGs) have been shown to be a practical solution for heat transfer enhancement with a low increase in pressure drop. LVGs can be punched, mounted or embossed on the fins. The longitudinal vortex (LV), which is generated when flow separates from the edges of the LVG, has its axis parallel to the main flow and has three potential mechanisms to improve heat transfer: developing boundary layers, swirl, and flow destabilization.

The first studies of LVGs aimed at heat transfer enhancement date from 1969, but it was in 1982 that Fiebig (1998) measured both heat transfer enhancement and pressure drop. Since then, many investigations of LVG have been carried out, where the principal parameters for their study are: quantity, position (relative to the heat exchanger and the angle of attack), and the aspect ratio of the LVG, kind of heat exchanger (tubes, fins, and position of the tubes), among others. Jacobi and Shah (1995) and Fiebig (1998) presented the state-of-the-art of LVGs focused on heat transfer enhancement. Among their conclusions, it was mentioned that

NOMENCLATURE

a	major diameter of Ellipse cases, m	p_s	span-averaged pressure, Pa
A_{min}	minimum flow cross-sectional area, m^2	P	perimeter of A_s, $2(9.1H + H)$, m
		$\dot{P}$	flow power consumption, W
A_T	total heat transfer surface area, m^2	Pr	Prandtl number, 0.7
A_s	flow cross-sectional area at entrance, m^2	$\dot{q}$	local heat flux, W/m^2
		$\dot{Q}$	total heat flux at heat exchanger area, W
b	minor radius of Ellipse cases, m	Re_{dh}	Reynolds number based on hydraulic diameter
B	transverse width of fins, m		
c_p	specific heat at constant pressure, kJ/kg·K	T	temperature, K
		T_b	bulk temperature, K
D_h	hydraulic diameter, $4A_s/P \approx 1.8H$, m	$\vec{u}$	velocity in the x, y, z directions; u, v, w, $m \cdot s^{-1}$
f	friction factor		
h	LVG height, m	**Greek Symbols**	
H	fin spacing, m		
j	Colburn factor		
k	thermal conductivity, W/m·K	α	thermal diffusivity, m^2/s
Nu	Nusselt number	β	angle of attack of LVG, deg
Nu_s	span-averaged Nusselt number	Δ	increment
Nu_m	averaged Nusselt number	ν	kinematic viscosity, m^2/s
p	pressure, Pa	ρ	density, kg/m^3

LVGs are more effective in laminar flow than in turbulent flow. Jacobi and Shah (1995) explained the theoretical basis of LVG and presented a critical review of the present studies and future needs.

The literature has few studies of LVG used in oval tube heat exchangers, for instance, Behle (1996), Chen et al. (1998a,b), Chu et al. (2009), Fiebig et al. (1994), Herpe et al. (2009), O'Brien et al. (2004), Prabhakar et al. (2003), Sohal and O'Brien (2001), Schulenberg (1996), and Tiwari et al. (2003). Oval tubes compared to round tubes have the advantage of delaying the flow separation on the tube surface, which is reflected in a smaller wake region, lower pressure drop, and a higher heat transfer rate (Schulenberg, 1996). In heat exchangers with a staggered tube arrangement and LVG, it is more advantageous to use oval or flat tubes rather than round ones, since they allow a larger trajectory for the LV and, therefore, a larger area of influence, before it is destroyed when colliding with the next tube. This is shown in the experimental study of Fiebig et al. (1994), where flat and round tubes in a staggered arrangement in a heat exchanger are compared.

There are also few studies in which the LVG geometry investigated is different, aside from triangular or rectangular shapes in the form of wings or winglets. In recent years, there have been investigations with some new LVG geometries, for instance, those of Gong et al. (2015), Gholami et al. (2014), Li et al. (2011), Lofti et al. (2014), Lin et al. (2015), Min et al. (2012), Zhou and Feng (2014), and Zhou and Ye (2012).

The purpose of this study is to compare different LVG geometries: delta and rectangular with other novel geometries obtained from Behle (1996) and Zhou and Feng (2014), in terms of heat transfer and pressure

drop in a plate fin and oval tube heat exchanger. The flow structure is studied in order to analyze the effect of LV on heat transfer enhancement. Computational Fluid Dynamics (CFD) software is used for a three-dimensional numerical solution of the Navier–Stokes and energy equations in the heat exchanger with and without LVG. The numerical model is compared with the simulations of Chen (1998) for validation. The potential impact of the LVG is quantified for possible applications.

Delta-type vortex generators have the best performance in laminar and transitional flow regions in a channel flow, while ellipse-shaped vortex generators have the best performance in fully turbulent regions due to the streamlined configuration and then the low pressure drop, which indicates the advantages of using this ellipse-shaped vortex generator for heat transfer enhancement in turbulent channel flow (Zhou and Feng, 2014). Spoon-type vortex generators have a better performance compared to delta-type vortex generators for transitional flow in a channel flow (Behle, 1996). The performance of delta-type compared to the ellipse-shaped and spoon-type vortex generators for laminar flow in a channel with oval tubes and conjugate heat transfer is not known, and it cannot be determined for previous results for plate flow and is, therefore, the motivation for the present investigation.

2. MODEL DESCRIPTION

2.1 Physical Model

An upper view of the plate fin and oval tube heat exchanger is shown in Fig. 1a. The fins have a width of 9.1*H*, a length of 15.4*H*, and a thickness of 0.06*H*, and the oval tube has a major radius of 6.4*H* and a minor

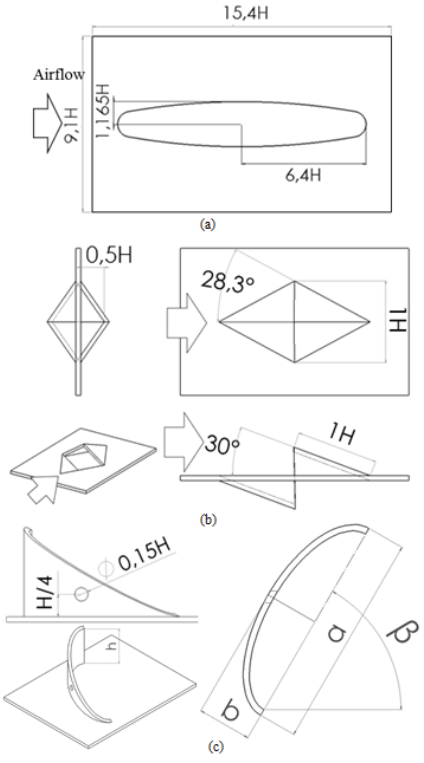

FIG. 1: Dimensions of: (a) heat exchanger, (b) LVG of the Spoon case, and (c) LVG of the Ellipse cases (the hole corresponds only to the Ellipse 5 case)

radius of 1.165*H*, where *H* is the separation between adjacent fins (10 mm). The cross section of the oval tube is formed by the connection of four arcs. The heat exchanger geometry is obtained from Chen (1998) and the chosen material is aluminum.

Eight different LVG geometries are studied: delta-type, rectangular, spoon-type, and ellipse-shaped. Their positions relative to the heat exchanger are shown in Fig. 2, where the eight cases of study are defined: Delta, Rectangular, Spoon, and Ellipse 1, 2, 3, 4, and 5, adding the Base case (heat exchanger without LVG). In the Delta and Rectangular cases, the LVG are punched out from the fin and have an angle of attack β equal

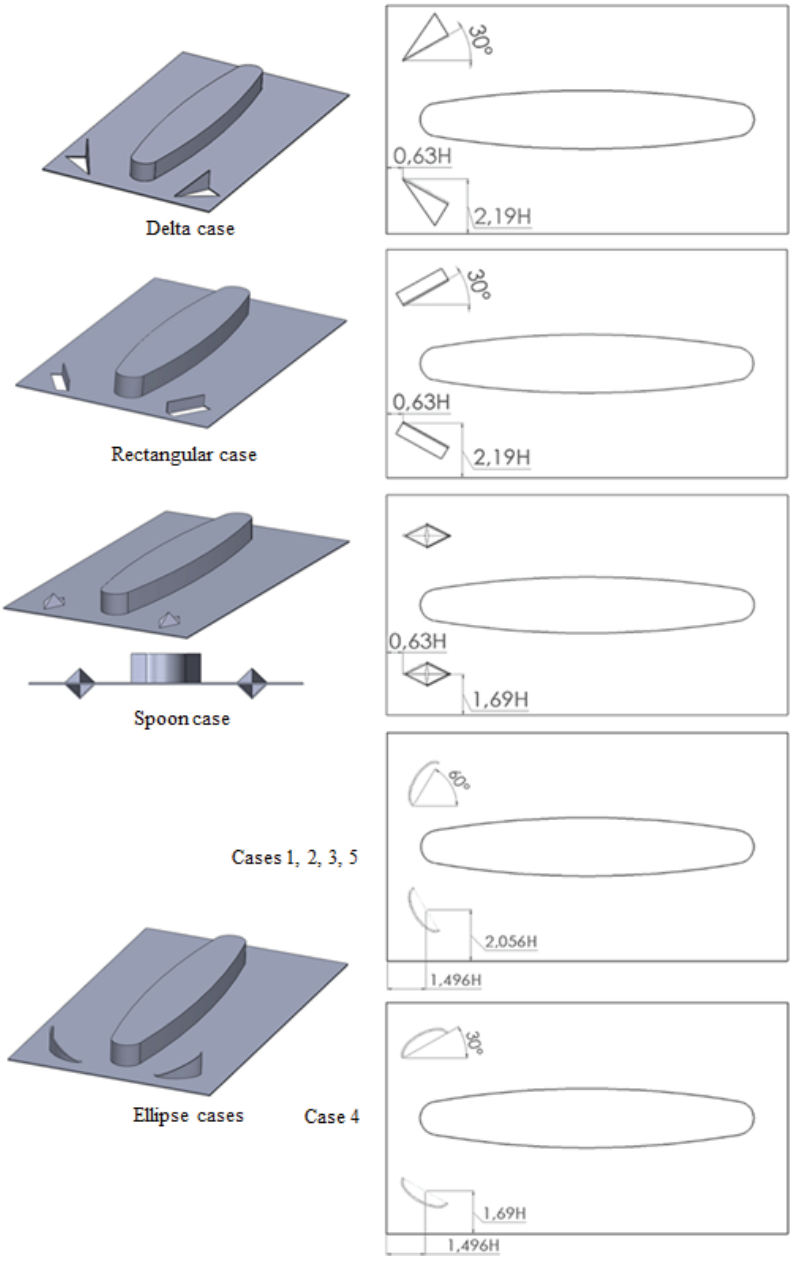

FIG. 2: Cases of study

to 30°. The delta-type LVG obtained from Chen (1998a) has a length of 2*H* and height *h* of *H*, while the rectangular LVG has a length of 2*H* and height *h* of 0.5*H*. The spoon-type LVG is formed by two identical protrusions, both punched out from the fin in opposite directions as shown in Fig. 1b. This LVG was experimentally studied by Behle (1996). The ellipse-shaped LVG, shown in Fig. 1c, was obtained from Zhou and Feng (2014), who performed an experimental investigation on different LVG geometries. In all Ellipse cases, the LVG is inserted on the fin and has a major diameter *a* equal to 2*H*. The parameters, which distinguish Ellipse cases from each other, are the minor radius *b*, height *h*, and the angle of attack β, which are shown in Table 1. The LVG of Ellipse 2 has a circular form, since *a*/2 is equal to *b*. Ellipse 5 has identical parameters to Ellipse 2 but has a 0.15*H* diameter hole perforated through its LVG and is located at 0.25*H* from the fin, in the middle of the ellipse, as indicated in Fig. 1c. In Table 2, the transverse area of each LVG is indicated.

Figure 3 presents the computational domain, which corresponds to the flow between two neighboring fins. The flow is described in an orthogonal system (*x*, *y*, *z*) with its origin at the entrance of the heat exchanger, as shown in Fig. 3, in which *x* is the streamwise coordinate, *y* is the spanwise direction, and *z* is the fin pitch coordinate. The two neighboring fins are taken as the upper and lower boundaries of the computational domain. The actual computational domain is extended 5*H* from the entrance to ensure a uniform velocity distribution. At the exit, the domain is extended 30*H* downstream to avoid recirculation and to ensure that the outflow boundary condition can be applied.

TABLE 1: Dimensional parameters of the Ellipse cases

Ellipse Cases	*b*	*h*	β	*a*
1	0.5*H*	1.0*H*	60°	2*H*
2	0.5*H*	0.8*H*	60°	2*H*
3	1.0*H*	0.8*H*	60°	2*H*
4	0.5*H*	1.0*H*	30°	2*H*
5 (hole)	0.5*H*	0.8*H*	60°	2*H*

TABLE 2: Transverse area of LVG

LVG	Transverse Area
Delta	$0.50H^2$
Rectangular	$0.50H^2$
Ellipse 1	$0.74H^2$
Ellipse 2	$0.59H^2$
Ellipse 3	$0.54H^2$
Ellipse 4	$0.41H^2$
Ellipse 5	$0.57H^2$
Spoon	$0.50H^2$

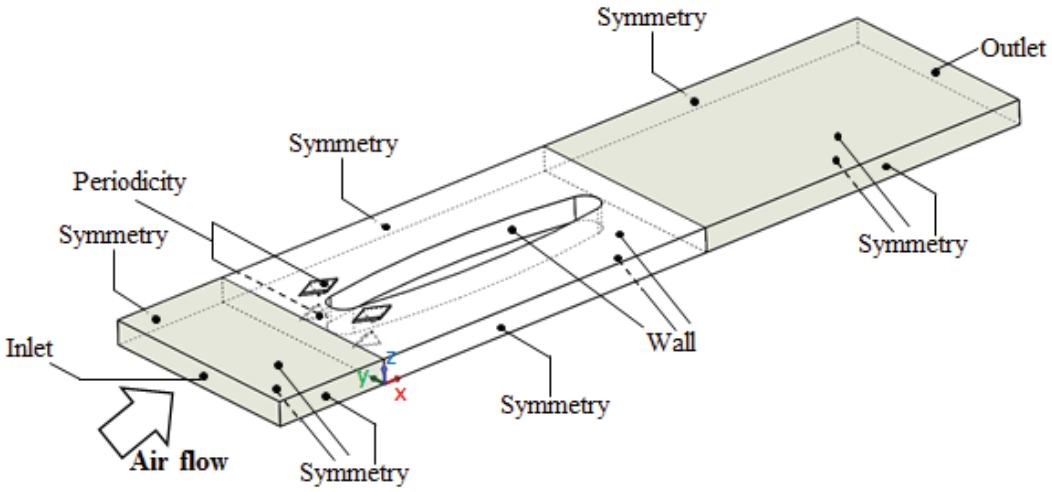

FIG. 3: Computational domain and boundary conditions

2.2 Governing Equations

The air is considered to be incompressible with constant properties. Due to the low air inlet velocity and the small space between the fins, the flow in the fin channel is assumed to be laminar and steady. The temperature of the tube surface is constant, while the temperature distribution in the fins is determined by solving the conjugated problem of heat transfer between the fluid and solid in the computational domain. The governing equations are:

continuity equation

$$\nabla \cdot \vec{u} = 0, \tag{1}$$

momentum equation

$$\vec{u} \cdot \nabla \vec{u} = -\frac{1}{\rho_a} \nabla p + \nu \nabla^2 \vec{u}, \tag{2}$$

energy equation

$$\vec{u} \cdot \nabla T = \alpha_a \nabla^2 T, \tag{3}$$

where $\vec{u}$, ρ, p, ν, T, and α represent the velocity vector, density, pressure, kinematic viscosity, temperature, and the thermal diffusivity, respectively. The subscript a refers to the air.

The temperature distribution in the fin is described by the two-dimensional heat conduction equation:

$$0 = \alpha_f \nabla^2 T_f + \frac{\dot{q}}{(\rho c_p)_f}. \tag{4}$$

Here the subscript f refers to the fin, c_p is the specific heat, and $\dot{q}$ is the heat transfer rate. In Eq. (4), q stands for the convective heat removal on both sides of the fin. This term couples the convective heat transfer to the fins and conductive heat transfer in the fins. The convective heat transfer is removed for the upper and lower sides of the fin.

2.3 Boundary Conditions

Figure 3 shows the boundary conditions for all surfaces, which are divided into the upstream and downstream extended regions as well as the heat exchanger region. In the upstream and downstream extended regions, the symmetry conditions hold. At the inlet boundary ($x = -5H$) the velocity and temperature are constant, $u = u_\infty$, $T = T_\infty = 293$ K. Four Re_{dh} are studied: 180, 360, 540, and 720. At the exit boundary ($x = 45.4H$), the streamwise gradients are zero. In the heat exchanger region, at the top and bottom fin boundaries and the tube surface, no-slip conditions are applied, shell conduction option is activated on the fin boundaries and a thickness of $0.03H$ is used, assuming adiabatic conditions on the external surface. On the tube surface, the temperature is constant and equal to 361 K. For the Delta, Rectangular, and Spoon cases, periodicity conditions are applied on the punched hole of the LVG. At the LVG boundaries, adiabatic and no-slip conditions are applied: the adiabatic boundary condition on the LVG is applied to simplify the conjugate heat transfer calculation on the fin and due to the LVG area being negligible compared to the fin area.

3. METHODOLOGY

3.1 Parameter Definition

The following parameters are defined to study the heat exchanger performance with and without LVG:

$$\mathrm{Re}_{dh} = \frac{u_\infty D_h}{\nu}, \tag{5}$$

$$f = \frac{2\Delta p}{\rho_a u_\infty^2} \frac{A_{\min}}{A_T}, \tag{6}$$

$$p_s(x) = \frac{\iint p(x, y, z)dydz}{\iint dydz}, \tag{7}$$

$$\mathrm{Nu}(x, y)\big|_{z=0,H} = \left(\frac{\dot{q}(x, y)\big|_{z=0,H}}{(T_f(x, y)\big|_{z=0,H} - Tb(x))} \right) \frac{D_h}{k_a}, \tag{8}$$

$$\mathrm{Nu}_s(x) = \frac{1}{B(x)} \int_0^{B(x)} \frac{\mathrm{Nu}(x, y)\big|_{z=0} + \mathrm{Nu}(x, y)\big|_{z=H}}{2} dy, \tag{9}$$

$$\mathrm{Nu}_m = \iint \frac{\mathrm{Nu}(x, y)\big|_{z=0} + \mathrm{Nu}(x, y)\big|_{z=H}}{2} dxdy, \tag{10}$$

$$\dot{q} = k_a \left. \frac{\partial T}{\partial z} \right|_{z=0,H}, \tag{11}$$

$$Tb(x) = \frac{\iint |u(x, y)|\, T(x, y, z)dydz}{\iint |u(x, y, z)|\, dydz}, \tag{12}$$

$$j = \frac{\mathrm{Nu}_m}{\mathrm{Re} \cdot \mathrm{Pr}^{1/3}}, \tag{13}$$

$$\dot{Q} = \iint_{A_T} \dot{q} dA_T , \tag{14}$$

$$\dot{P} = u_\infty \cdot A_s \cdot \Delta p . \tag{15}$$

3.2 Grid Generation Technique and Independence

A three-dimensional grid system is established for the computational domains using the software ANSYS 14.5. The computational domain is divided into three subdomains, and different strategies are employed for each subdomain to generate the mesh, as shown in Fig. 4. For the extended domains, a structured hexahedral mesh is employed. The heat exchanger domain is meshed using unstructured tetrahedral elements with the advanced size function: proximity and curvature. Mesh independency is performed for the Delta case, Re_{dh} = 720. Table 3 shows the results of Nu_m and f for three meshes: 870,000, 1,280,000, and 1,770,000 elements. The differences in Nu_m and f between meshes 1,280,000 and 1,770,000 are 1.2% and 0.2%, respectively. Due to the low differences in the results, and in order to minimize the computation time, the 1,280,000 mesh was adopted.

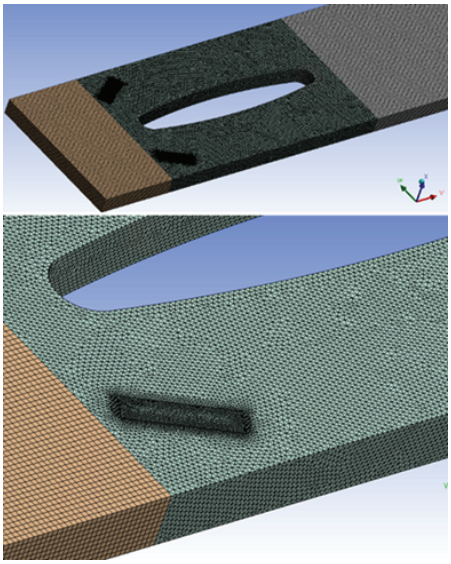

FIG. 4: Mesh (rectangular case)

TABLE 3: Results of different grid sizes

Grid Size	870,000	1,280,000	1,770,000
Nu_m	12.57	12.38	12.23
f	0.0883	0.0881	0.0883

3.3 Numerical Method and Validation

Equations (1)–(4) are solved by the finite volume method from the software ANSYS Fluent 14.5. The SIMPLEC algorithm is used for the pressure–velocity coupling. A second-order upwind scheme is used for spatial discretization of pressure, momentum, and energy, and the Green–Gauss node-based scheme is used for gradient determination. The average vertex values of velocity, temperature, and heat transfer rate are evaluated in different vertex points of the heat exchanger, as well as the area-weighted average of the heat transfer rate in the fins for each iteration of simulations. The convergence of simulations is determined by the convergence of these terms, with a convergence criterion of 10^{-6}. The time step is 0.0005 s with maximum 20 iterations in each time step; the convergence criterion in each time step is set to 10^{-3} for the momentum equations, and to 10^{-6} for the energy equation. The conjugated problem converged in 25 s. The results for the Delta case are compared to the numerical results of Chen (1998), shown in Figs. 5 and 6. These figures show that the maximum discrepancies of the average Nusselt number Nu_m and the friction factor f are 6% and 5%, respectively, which indicates the reliability of the computational model.

In order to validate the numerical method, a comparison of the present results with the experimental data reported by Valencia (1993), Lotfi et al. (2014), and Chu et al. (2009) for the Base case without LVG was performed. The experimental results for the first row of the plate fin and oval tube heat exchanger presented by Valencia (1993) were used. The numerical results validated with experimental data presented by Lotfi et al. (2014) and Chu et al. (2009) for a smooth wavy fin and an elliptical tube, and a plate fin and an elliptical tube, respectively, were compared. The results of Nusselt numbers were extrapolated to the Reynolds numbers used in the present investigation and shown in Fig. 7. The maximum difference between the present numerical results obtained by laminar flow and the experimental results of Valencia (1993) was 11%, at Re_{dh} = 180. Comparing the results of Lotfi et al. (2014) and Chu et al. (2009), the maximum difference in the Nusselt numbers was 20%. The agreement between the numerical results and

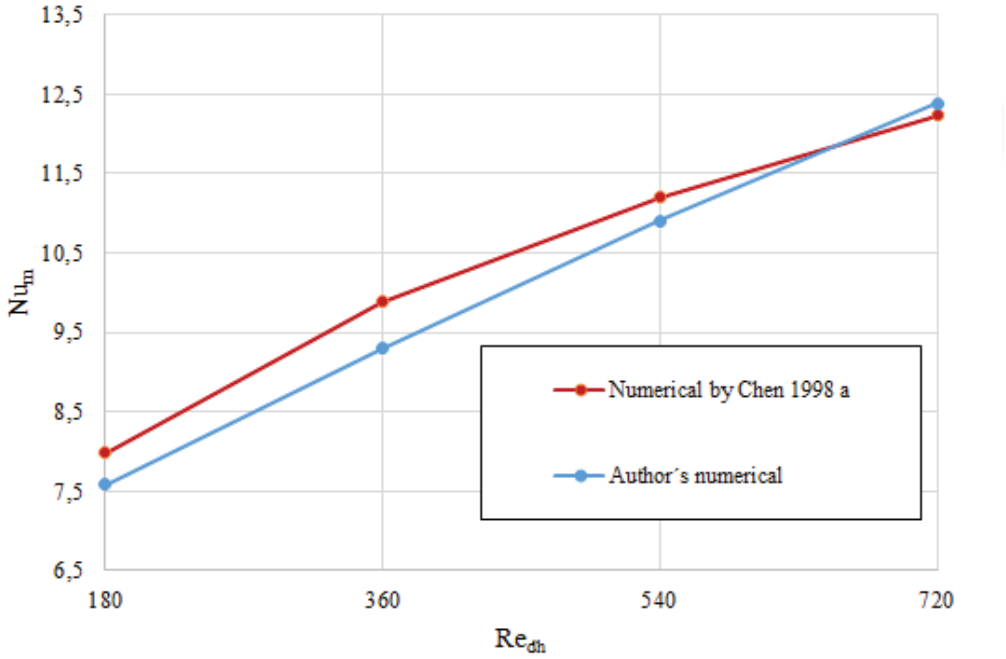

FIG. 5: Numerical comparison of Nu_m for model validation for the Delta case

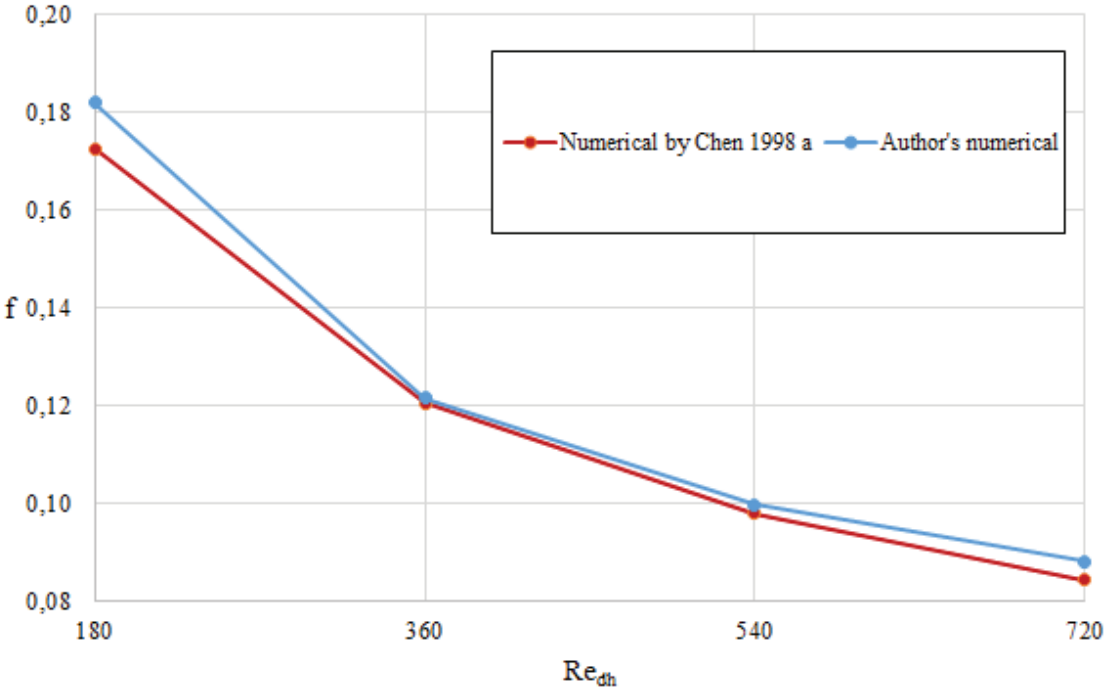

FIG. 6: Numerical comparison of friction factor for model validation for the Delta case

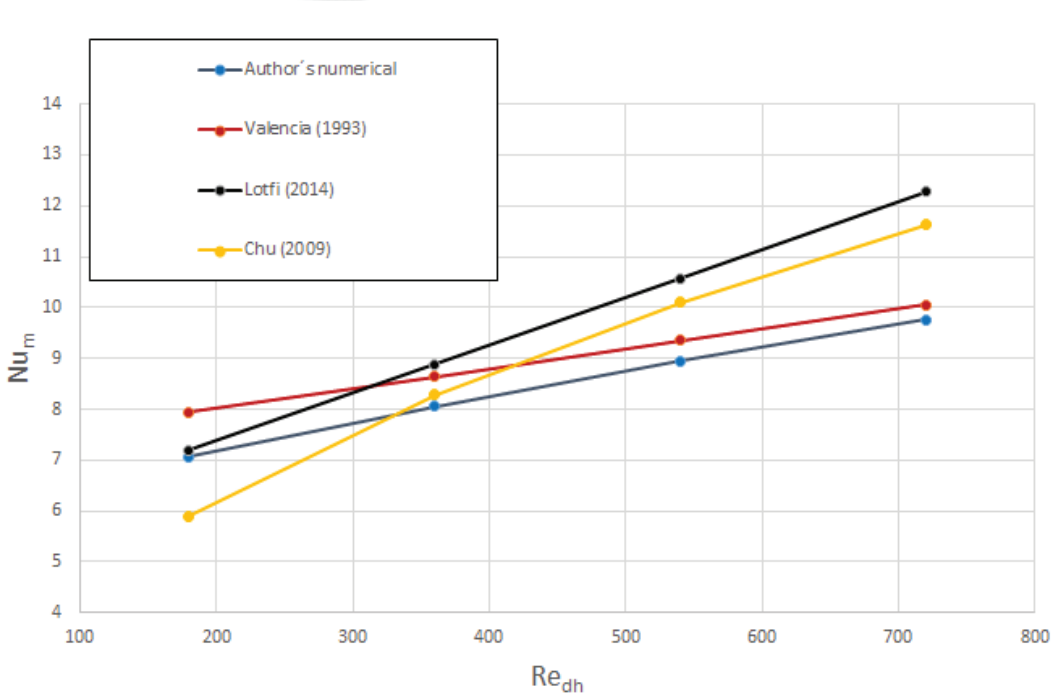

FIG. 7: Comparison of Nu_m with experimental results for the Base case

experimental data is reasonable and confirms the reliability of the computational model. The published experimental data for a plate fin and tube heat exchanger are in the transitional or turbulent flow and, therefore, a comparison for laminar flow modeling is not direct to perform. The geometries used by Lotfi et al. (2014) and Chu et al. (2009) were different from those used in the present investigation, and that is another possible reason for the difference between the reported Nusselt numbers.

4. RESULTS AND DISCUSSION

4.1 Flow Structure

For all cases, the flow structure is characterized by the presence of an LV product of the interaction with LVG. When flow enters the heat exchanger and strikes the LVG, flow separation from the LVG edges occurs due to the pressure variation between the front and back of the LVG, generating the LV. The three-dimensional streamline from Fig. 8 shows this phenomenon, where flow separates from the LVG leading edge in the Rectangular case.

Figure 9 shows the velocity vectors v and w in different Y–Z sections through the x axis. It can be observed that, for all cases, except for the Spoon case, one LV is formed for each LVG, and it propagates along the x axis. For the Spoon case, two LVs are formed for each LVG, as Behle (1996) indicated, which are not symmetrical because of the deviation caused by the tube. For the Delta, Rectangular, and Spoon cases, a fraction of the flow goes through the punched hole in the fins and becomes part of the LV.

Through the velocity vectors shown in Fig. 9, it can be observed that the intensity of the LV varies between the cases. The Delta, Rectangular, and Ellipse 1 cases show the highest intensity, followed by the Ellipse 2 and Ellipse 5 cases (both with similar intensities), Ellipse 3, Ellipse 4, and Spoon cases with the lowest intensities, in which the LV seems to dissipate before it leaves the heat exchanger. For all cases, the LV weakens as it propagates along the x axis. In particular, for the Ellipse cases, there is agreement between the intensity of the LV and the transverse area, illustrated in Table 2. If the former increases, the latter does as well. The Ellipse 1 case, with the highest transverse area ($0.74H^2$), has the highest intensity, followed by the Ellipses 2 ($0.59H^2$) and Ellipse 5 ($0.57H^2$) cases, which have a smaller height h than the Ellipse 1 case. The order continues with the Ellipse 3 ($0.54H^2$) case, although its LVG geometry differs from the other Ellipse cases (it has a circular shape); so the comparison only in terms of the transverse area would be insufficient. Finally, the Ellipse 4 case has both the lowest intensity and transverse area ($0.41H^2$) because its LVG has a smaller angle of attack (30^o) than the rest (60^o). The velocity vectors in Fig. 8 for the eight vortex generators were plotted using the same scale; therefore, the sizes of the arrows for different vortex generators represent the vorticity in different planes. The magnitude of the velocity is the inlet velocity in the plane $x/H = 1.5$ of Fig. 8 for the eight vortex generators.

4.2 Thermal Behavior

To study the implications of the LVG on the thermal behavior of the heat exchanger, Fig. 10 shows the comparison of the Delta and Base cases in the Y–Z section $x/H = 7.7$ (the middle of the heat exchanger). Figure 10a shows the velocity vectors tangential to the section of the Delta case, where the aforementioned LV is observed with its core at $y/H \approx 1.3$ and $z/H \approx 0.5$, and a counterclockwise case. The LV introduces a secondary flow that promotes the mixture. This can be seen through the temperature contours (shown in Fig. 10b,c) of the Delta and Base cases, respectively. In the Base case, the flow near the fins and tube always has the highest temperature. However, in the Delta case, the flow between the fins in the LV zone shows a

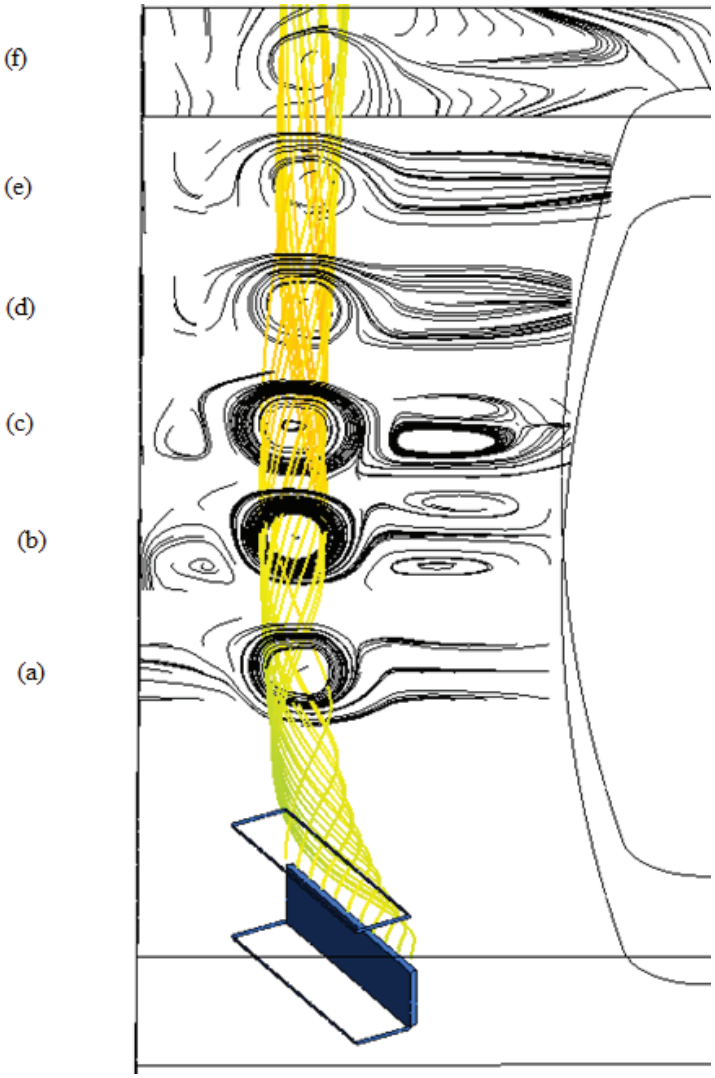

FIG. 8: Two-dimensional streamlines (in black) for *Y–Z* sections at: (a) $x/H = 5.5$, (b) $x/H = 7.7$, (c) $x/H = 9.5$, (d) $x/H = 11.5$, (e) $x/H = 13.5$, and (f) $x/H = 15.4$, and three-dimensional streamlines (in color) starting from the leading edge of the LVG for the Rectangular case ($Re_{dh} = 540$)

higher temperature due to the mixture. Aside from the enhanced mixture of the flow, the thermal layer is also disturbed by the LV. Indeed, in the lower fin, the thermal layer thins and thickens at $y/H \approx 1.8$ and $y/H \approx 0.8$, respectively, while in the upper fin it is the other way round. The quantified effect of LV on heat transfer is shown in Fig. 10d, where the Nusselt number ratio between the Delta and Base cases is plotted through the y axis (at $x/H = 7.7$) for the lower fin. It is observed that the heat transfer rate increases in the thinned zone, reaching a maximum of $Nu_{Delta}/Nu_{Base} = 1.9$ at $y/H \approx 1.8$, while it decreases in the thickened zone, with a minimum equal to 0.7 at $y/H \approx 0.8$. The increase in the heat transfer rate is, however, notoriously greater than the decrease. On the other hand, a slight increase in the heat transfer rate is observed in the zones not directly affected by the LV.

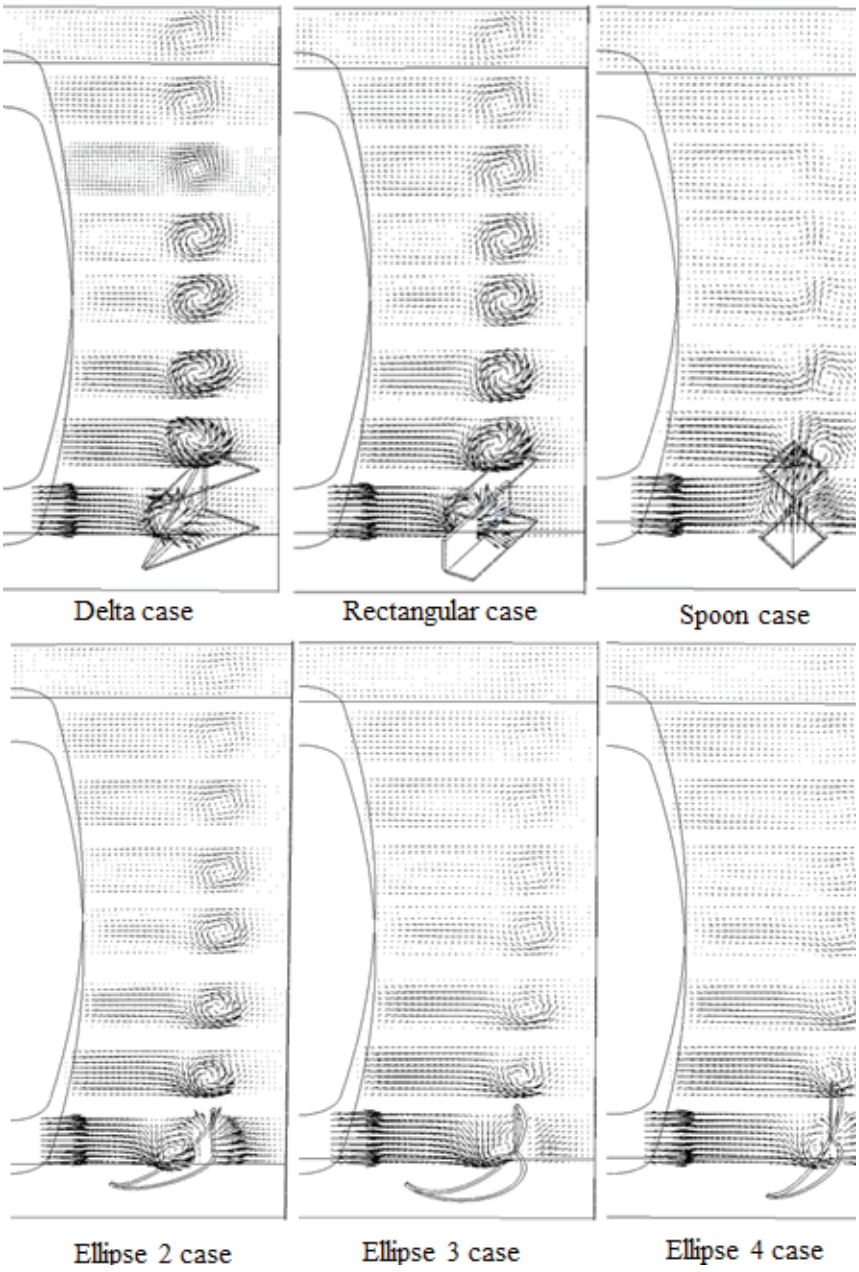

FIG. 9: Velocity vectors (Re_{dh} = 540) tangential to *Y–Z* sections at: (a) x/H = 1.5, (b) x/H = 3.5, (c) x/H = 5.5, (d) x/H = 7.7, (e) x/H = 9.5, (f) x/H = 11.5, (g) x/H = 13.5, and (h) x/H = 15.4

4.3 Case Comparison

As shown in Fig. 9, the intensity of LV varies between cases, so the heat transfer rates along fins could also be different between cases. Figure 11 shows the span-averaged Nusselt number Nu_s along the *x* axis for the Base, Delta, and Spoon cases for Re_{dh} = 720. It is observed that heat transfer enhancement starts when LVs are formed (Delta and Spoon cases), and it is maintained along the *x* axis (which is an important property

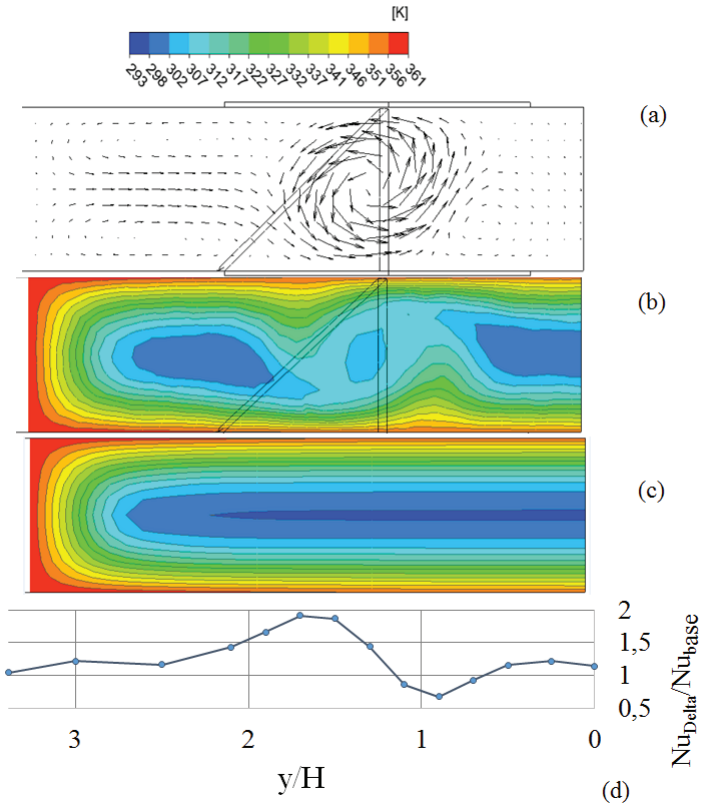

FIG. 10: Comparison between the Delta and Base cases (Re_{dh} = 540) at *Y–Z* section x/H = 7.7: (a) velocity vectors tangential to the section of the Delta case, (b) and (c) temperature contours of the Delta and Base cases, respectively, and (d) Nusselt number ratio (lower fin) between the Delta and Base cases along the *y* axis

of LV), compared to the Base case. On the other hand, the Delta case causes a higher enhancement than the Spoon case, in agreement with its higher intensity of the LV.

Figure 12 shows the percentage change in the heat transfer rate in the LVG cases compared to the Base case, at the same Re_{dh}. There is an increase in all cases and it becomes higher as Re_{dh} increases. The Delta case shows, in general, the highest increase (14% for Re_{dh} = 720), followed by the Ellipse 1 (13%) and Ellipse 2, Ellipse 5, and Rectangular cases with similar results (11%). The cases with the lowest vortex intensity show the lowest increase in the heat transfer rate; the Ellipse 3 (8%) case is followed by the Ellipse 4 and Spoon cases with similar results (7%). The Ellipse 5 case has similar results on the heat transfer rate compared to the Ellipse 2 case; therefore, the perforated hole in its LVG is irrelevant.

Figure 13 shows the percentage change in the pressure drop of the LVG cases compared to the Base case, at the same Re_{dh}. There is an increase in all cases and it becomes higher as Re_{dh} increases. The increase in the pressure drop is due to the collision of the flow with the LVG and the friction of the LV with the surface of the fins. Chen et al. (1998a) showed that the major cause of pressure drop is collision rather than friction, which is negligible when compared to the heat exchanger without LVG. The difference in the pressure drop between the cases is fairly constant for all Re_{dh}. The Ellipse 1 case has the highest increase in the pressure drop (20% for Re_{dh} = 720), followed by the Delta (19%), Ellipse 2 (15%), Ellipse 5 (14%), Rectangular (13%), Ellipse 3 (11%), and Ellipse 4 and Spoon (9% both) cases.

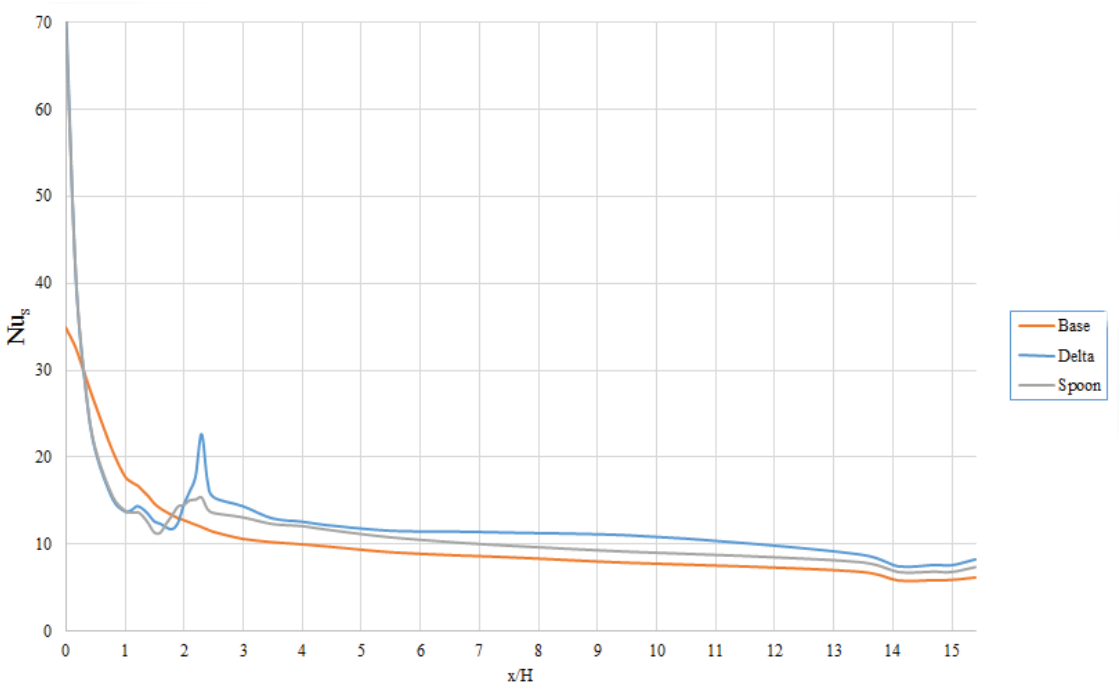

FIG. 11: Span-averaged Nusselt number Nu_s along the x axis for the Base, Delta, and Spoon cases (Re_{dh} = 720)

Many performance evaluation criteria have been developed in order to study the heat transfer enhancement mechanisms, some of them described by Webb (1981). In this study, the plot from Fig. 14 is used, where the curves of the heat transfer rate [Eq. (14)] as a function of flow power consumption [given by Eq. (15)] are shown. The curve of the Base case is constructed at Re_{dh} equal to 180, 270, 360, 450, 540, 630, 720, and 810. The curves show that under the same power consumption there is an increase in the heat transfer rate compared to the Base case. Three groups of curves are distinguished in terms of heat transfer performance:

1) the curve of the Base case, which has the lowest heat transfer rate,
2) the curves of the Ellipse 3, Ellipse 4, and Spoon cases, which have the lowest increase in the heat transfer rate compared to the Base case,
3) the curves of the Delta, Rectangular, Ellipse 1, Ellipse 2, and Ellipse 5 cases, which have the highest increase in the heat transfer rate.

Therefore, the third family shows the best performance. Moreover, considering that LVGs of the Delta and Rectangular cases are easier to manufacture, these cases prove to be more attractive.

The Base case represents a finned heat exchanger with an oval tube, and for laminar flow the technique of heat transfer enhancement with longitudinal vortex generator produces limited improvements. Delta-type vortex generators have shown a large heat transfer enhancement in a plate fin heat exchanger with oval tubes (Fiebig et al., 1994). Zhou and Feng (2014) showed that ellipse-shaped vortex generators have the best performance in fully turbulent regions, while spoon-type vortex generators have a better performance for transitional flow in a channel flow (Behle, 1996). The comparison of eight different geometries of vortex generators, including the conjugate heat transfer on the fin and the interaction with the oval tube for laminar flow conditions, is the most important contribution of this investigation. The delta-type, rectangular, and three

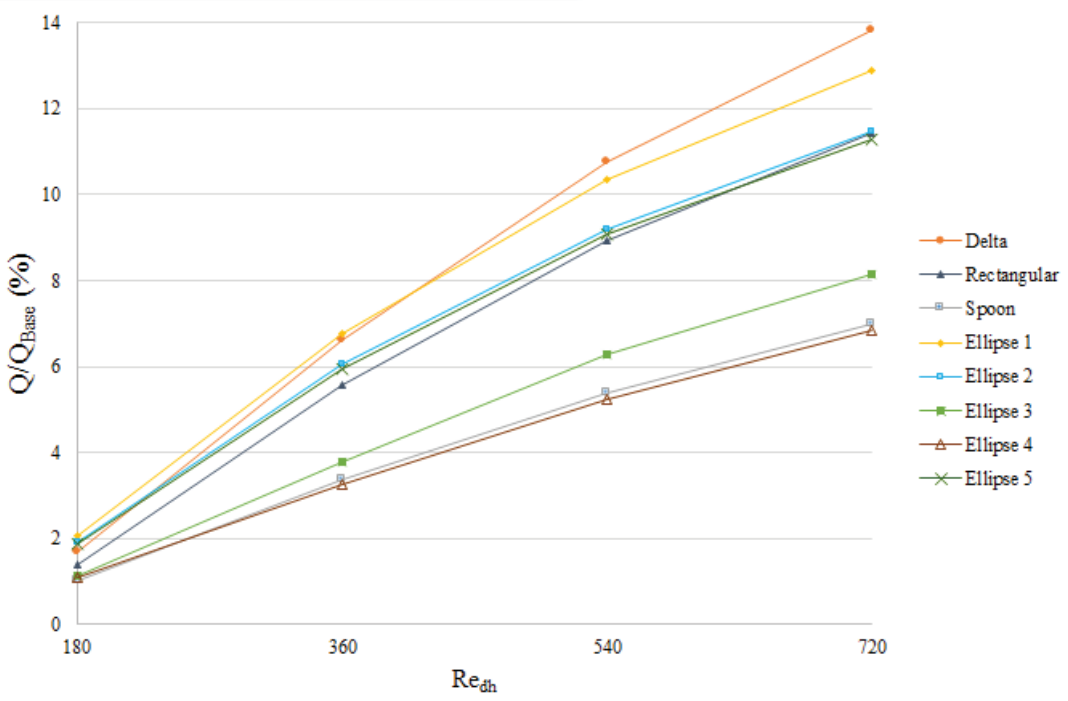

FIG. 12: Increase in the heat transfer rate of the LVG cases compared to the Base case

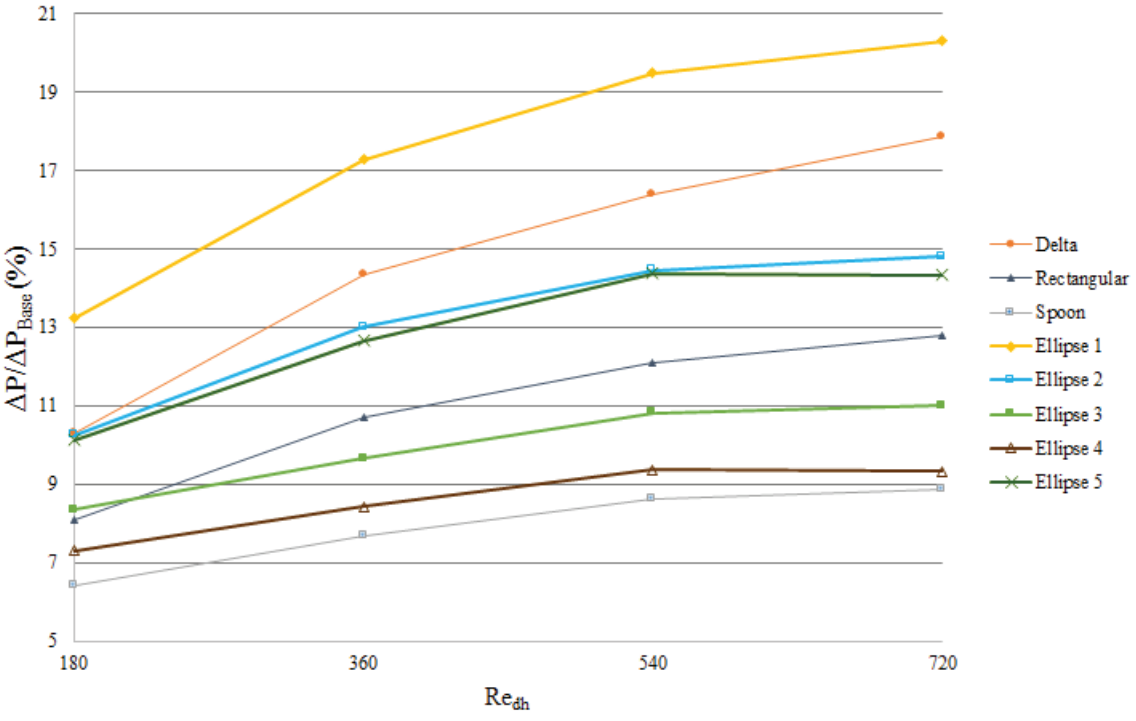

FIG. 13: Increase in the pressure drop of the LVG cases compared to the Base case

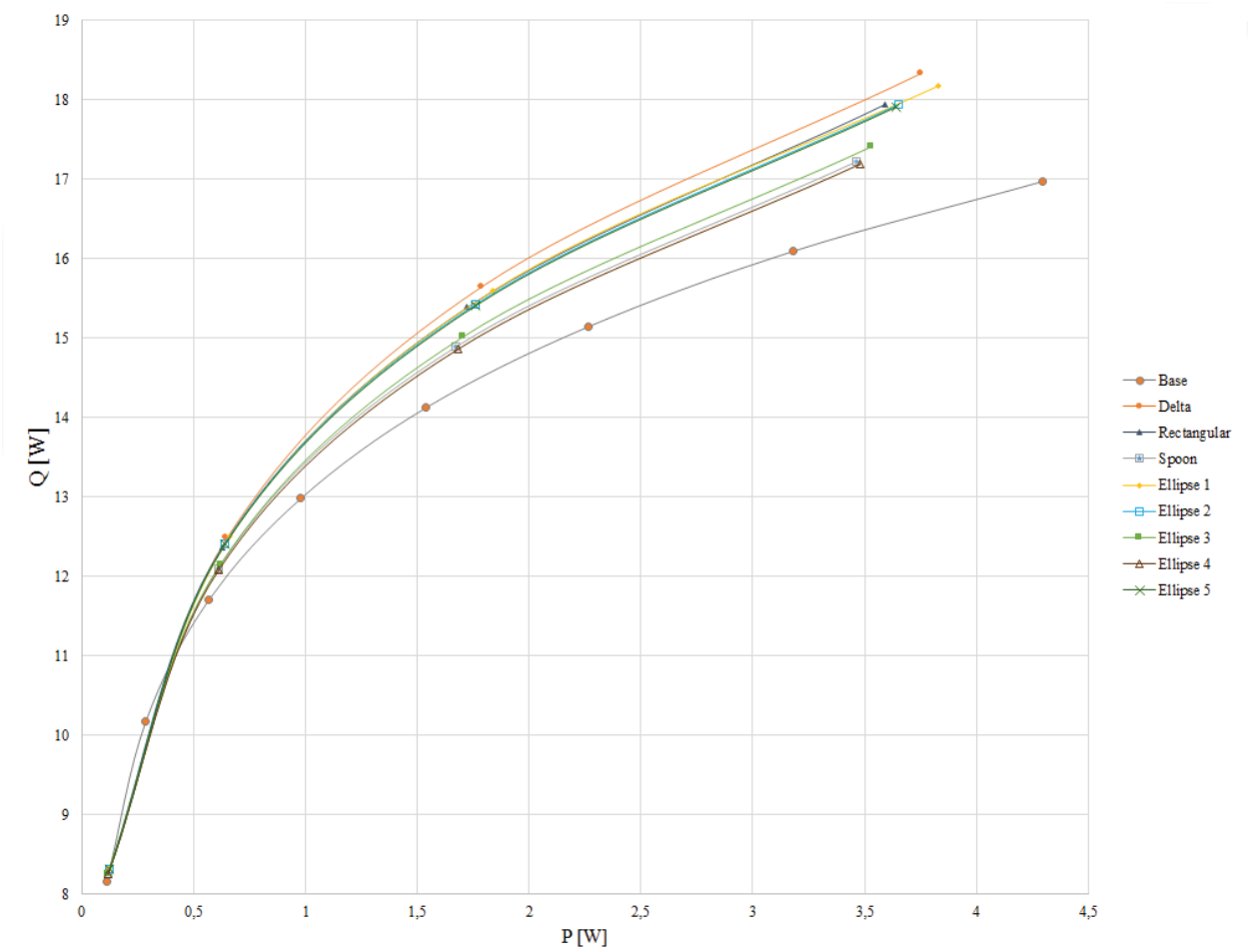

FIG. 14: Heat transfer as a function of flow power consumption

ellipse-shaped vortex generators have a similar increase in the heat transfer rate for the same flow power consumption.

5. CONCLUSIONS

Three-dimensional numerical simulations have been performed to study the flow and heat transfer in a plate fin and oval tube heat exchanger. Besides the Base case (heat exchanger without LVG), eight cases are studied where the LVG geometry is varied (i.e., Delta, Rectangular, Spoon, and Ellipse 1, 2, 3, 4, and 5).

The flow structure of the Delta, Rectangular, and Ellipse cases is characterized by the presence of one LV for each LVG and two LVs for the Spoon case. The intensity of the LV varies between cases; Delta, Rectangular and Ellipse 1 have the highest intensity, followed by Ellipse 2 and 5 and, finally, Ellipse 3 and 4, and Spoon, in which the LV seems to dissipate before exiting the heat exchanger.

All cases with LVG show an increase in heat transfer compared to the Base case, for all Re_{dh}. The Delta case shows, in general, the highest increase (14% for Re_{dh} = 720), while the Ellipse 4 and Spoon cases show

the lowest increase (7%), which is in agreement with their vortex intensity. The Ellipse 2 and Ellipse 5 cases show no practical differences in heat transfer and pressure drop performances; therefore, the hole in LVG of the Ellipse 5 case has no relevance. The highest increases in heat transfer, under the same power consumption, correspond to the Delta, Rectangular, Ellipse 1, 2, and 5 cases.

ACKNOWLEDGMENT

This work was partially supported by Grant PFB03 2007 CMM, Universidad de Chile, CONICYT, Chile.

REFERENCES

Behle, M., Wärme- und Strömungs technische Untersuchung stanzgeprägter Hutzen als Längswirbelerzeuger, PhD, Ruhr-Universität Bochum, 1996.

Chen, Y., Leistungssteigerung von Wärmeübertragern mit berippten Ovalrohren durch Längswirbelerzeuger, PhD, Ruhr-Universität Bochum, 1998.

Chen, Y., Fiebig, M., and Mitra, N.K., Conjugate heat transfer of a finned oval tube with a punched longitudinal vortex generator in form of a delta winglet-parametric investigations of the winglet, *Int. J. Heat Mass Transfer,* vol. **41**, pp. 3961–3978, 1998a.

Chen, Y., Fiebig, M., and Mitra, N.K., Heat transfer enhancement of a finned oval tube with punched longitudinal vortex generators in-line, *Int. J. Heat Mass Transfer,* vol. **41**, pp. 4151–4166, 1998b.

Chu, P., He, Y., Lei, Y., Tian, L., and Li, R., Three-dimensional numerical study on fin-and-oval-tube heat exchanger with longitudinal vortex generators, *Appl. Thermal Eng.,* vol. **29**, pp. 859–876, 2009.

Fiebig, M., Vortices, Generators and heat transfer, *Trans. IChemE,* vol. **76**, pp. 108–123, 1998.

Fiebig, M., Valencia, A., and Mitra, N., Local heat transfer and flow losses in fin-and-tube heat exchangers with vortex generators: A comparison of round and flat tubes, *Exp. Thermal Fluid Sci.,* vol. **8**, pp. 35–45, 1994.

Gong, B., Wang, L., and Lin, Z., Heat transfer characteristics of a circular tube bank fin heat exchanger with fins punched curve rectangular vortex generators in the wake regions of the tubes, *Appl. Thermal Eng.,* vol. **75**, pp. 224–238, 2015.

Gholami, A., Wahid, M., and Mohammed, H., Heat transfer enhancement and pressure drop for fin-and-tube compact heat exchangers with wavy rectangular winglet-type vortex generators, *Int. Commun. Heat Mass Transfer,* vol. **54**, pp. 132–140, 2014.

Herpe, J., Bougeard, D., Russeil, S., and Stanciu, M., Numerical investigation of local entropy production rate of a finned oval tube with vortex generators, *Int. J. Thermal Sci.,* vol. **48**, pp. 922–935, 2009.

Jacobi, A. and Shah, R., Heat transfer surface enhancement through the Use of longitudinal vortices: A review of recent progress, *Exp. Thermal Fluid Sci.,* vol. **11**, pp. 295–309, 1995.

Li, J., Wang, S., Chen, J., and Lei, Y., Numerical study on a slit fin-and-tube heat exchanger with longitudinal vortex generators, *Int. J. Heat Mass Transfer,* vol. **54**, pp. 1743–1751, 2011.

Lin, Z., Liu, C., Lin, M., and Wang, L., Numerical study of flow and heat transfer enhancement of circular tube bank fin heat exchanger with curved delta-winglet vortex generators, *Appl. Thermal Eng.,* vol. **88**, pp. 198–210, 2015.

Lotfi, B., Min, Z., Sundén, B., and Qiuwang, W., 3D numerical investigation of flow and heat transfer characteristics in smooth wavy fin-and-elliptical tube heat exchangers using new type vortex generators, *Energy,* vol. **73**, pp. 233–257, 2014.

Min, C., Qi, C., Wang, E., Tian, L., and Qin, Y., Numerical investigation of turbulent flow and heat transfer in a channel with novel longitudinal vortex generators, *Int. J. Heat Mass Transfer,* vol. **55**, pp. 7268–7277, 2012.

O'Brien, J., Sohal, M., and Wallstedt, P., Local heat transfer and pressure drop for finned-tube heat exchangers using oval tubes and vortex generators, *J. Heat Transfer,* vol. **126**, pp. 826–835, 2004.

Prabhakar, V., Biswas, G., and Eswaran, V., Numerical prediction of heat transfer in a channel with a built-in oval tube and various arrangements of the vortex generators, *Numer. Heat Transfer, Part A,* vol. **44**, pp. 315–333, 2003.

Schulenberg, F., Finned elliptical tubes and their application in air-cooled heat exchangers, *J. Eng. Ind.,* vol. **88**, pp. 179–186, 1996.

Sohal, M. and O'Brien, J., Improving air-cooled condenser performance using winglets and oval tubes in a geothermal power plant, *Geothermal Resources Council Trans.,* vol. **25**, pp. 607–610, 2001.

Tiwari, S., Maurya, D., Biswas, G., and Eswaran, V., Heat transfer enhancement in cross-flow heat exchangers using oval tubes and multiple delta winglets, *Int. J. Heat Mass Transfer,* vol. **46**, pp. 2841–2856, 2003.

Valencia, A., Wärmeübergang und Druckverlust in Lamellen-Rohr-Wärmeübertragern mit Längswirbelerzeugern, PhD, Ruhr-Universität Bochum, 1993.

Webb, R.L., Performance evaluation criteria for use of enhanced heat transfer surfaces in heat exchanger design, *Int. J. Heat Mass Transfer,* vol. **24**, pp. 715–726, 1981.

Zhou, G. and Feng, Z., Experimental investigations of heat transfer enhancement by plane and curved winglet type vortex generators with punched holes, *Int. J. Thermal Sci.,* vol. **78**, pp. 26–35, 2014.

Zhou, G. and Ye, Q., Experimental investigations of thermal and flow characteristics of curved trapezoidal winglet type vortex generators, *Appl. Thermal Eng.,* vol. **37**, pp. 241–248, 2012.